

CrystEngComm

Accepted Manuscript



This is an *Accepted Manuscript*, which has been through the Royal Society of Chemistry peer review process and has been accepted for publication.

Accepted Manuscripts are published online shortly after acceptance, before technical editing, formatting and proof reading. Using this free service, authors can make their results available to the community, in citable form, before we publish the edited article. We will replace this *Accepted Manuscript* with the edited and formatted *Advance Article* as soon as it is available.

You can find more information about *Accepted Manuscripts* in the [Information for Authors](#).

Please note that technical editing may introduce minor changes to the text and/or graphics, which may alter content. The journal's standard [Terms & Conditions](#) and the [Ethical guidelines](#) still apply. In no event shall the Royal Society of Chemistry be held responsible for any errors or omissions in this *Accepted Manuscript* or any consequences arising from the use of any information it contains.



Journal Name

ARTICLE

One step ionic liquid assisted ultrasonic method for preparation of BiOCl/m-BiVO₄ heterojunctions with enhanced visible light photocatalytic activity

Received 00th January 20xx,
Accepted 00th January 20xx

DOI: 10.1039/x0xx00000x

www.rsc.org/

Chengyu Yang,^a Feng Li^a and Taohai Li^{a*}

By combining the advantages of both of ionic liquids and ultrasound, a novel method namely ionic liquid assisted ultrasonic method was developed to prepare BiOCl/m-BiVO₄ heterojunctions in several hours at room temperature. Through this method, BiOCl/BiVO₄ heterojunctions with different contents of BiOCl can be conveniently synthesized via the simple change of the amount of 1-butyl-3-methylimidazolium chloride [EMIM]Cl used during the preparation process. The X-ray diffraction, X-ray photoelectron spectroscopy, and energy-dispersive X-ray spectroscopy were used to demonstrate the structures of the as-prepared BiOCl/m-BiVO₄ heterojunctions. And the morphologies were characterized via scanning electron microscopy and transmission electron microscopy. The results suggest that the as-prepared BiOCl/m-BiVO₄ heterojunctions have high photocatalytic activity and stability for the degradation Rhodamine B both under visible light and sunlight irradiation at room temperature. Moreover, a possible mechanism was proposed.

Introduction

Semiconductor photocatalyst is an economic and environmentally friendly option for environmental protection, which has attracted intense research interest owing to the utilization of natural solar energy without secondary pollution.¹⁻⁴ Among these, monoclinic BiVO₄ as a semiconductor photocatalyst has been attracted widely attention for photochemical processes because of its narrow band gap and excellent photocatalytic performance.⁵⁻⁷ However, the wide application of BiVO₄ in the fields of solar conversion and environmental purification are restricted by its poor separation efficiency of photogenerated electrons and holes and poor electrical conductivity and adsorptive performance.⁸⁻¹⁰ As a result, many attempts have been made to improve the photocatalytic activity of BiVO₄, which include controlling the morphologies,¹¹⁻¹² noble metal loading,¹³⁻¹⁴ and semiconductor combination.¹⁵⁻¹⁶

It has been reported that the formation of heterojunction can speed up the separation rate of photogenerated electrons and holes and reduce their recombination, thus increasing the photo-quantum efficiency.¹⁷⁻¹⁸ So far, a lot of semiconductors with narrow band-gap, such as Bi₂O₃,¹⁹ V₂O₅,²⁰ Bi₂O₂CO₃,²¹ and CuO,²² have been investigated to couple with BiVO₄. However, as we all know, only the semiconductors with suitable energy band structure can improve the charge separation efficiency

and then enhance the photocatalytic activity of m-BiVO₄. BiOCl is an acceptable n-type semiconductor with wide-band-gap ($E_g = 3.5$ eV).²³⁻²⁴ A p-n heterojunction can be easily formed via the combination of the p-type BiVO₄ and the n-type BiOCl, which can build an internal electric field and provide a potential driving force.²⁵ As a result, the probability of separation efficiency of photogenerated electrons and holes is enhanced and the recombination of photogenerated charge carriers is reduced.

Sonochemistry is a result of acoustic cavitation, which includes formation, growth, and implosive collapse of bubbles in liquids.²⁶ The bubble collapse produces intense local heating, high pressures, and very short lifetimes. The localized hot spots drive high-energy for chemical reactions,²⁷ such as oxidation, reduction, dissolution, and decomposition. In the recent years, ultrasonic synthesis method has attracted considerable attention owing to its facile, highly efficient and environmentally friendly properties.²⁸⁻³⁰ To minimize the solvent vapor and maximize the temperatures reached to bubbles during acoustic cavitation, the ultrasonic synthesis of materials usually use the solvents with high boiling point.³³ Ionic liquids (ILs) are room temperature molten salts, which have been widely used for the synthesis of inorganic nanomaterials due to its unique properties, such as high thermal stability and ionic conductivity, excellent dissolving ability, wide electrochemical window, and negligible vapor pressure.³²⁻³⁴ Therefore, it is urgent and important to combining the advantages both of ILs and ultrasound to synthesis materials.

Up to now, only two methods have been reported to synthesize BiOCl/m-BiVO₄ heterojunction photocatalysts, which are hydrothermal method³⁵ and deposition-

^aCollege of Chemistry, Key Lab of Environment Friendly Chemistry and Application in Ministry of Education, Xiangtan University, Xiangtan, 411105, China. Fax: 86-731-58292251; Tel: 86-731-58292206; E-mail: hnlth@xtu.edu.cn

† Electronic Supplementary Information (ESI) available: [the pore-size distributions of all samples]. See DOI: 10.1039/x0xx00000x

precipitation method.³⁶ The prepared BiOCl/m-BiVO₄ heterostructures showed a certain photocatalytic performance because of the improvement of photogenerated electron–hole separation and the enhancement of the interfacial charge transfer efficiency. However, both of the two methods were complex, and higher reaction temperature and longer reaction time are always needed. Moreover, additional steps and reagents are necessary for preparing the pure BiVO₄. Therefore, it is much desired to develop a simple method to prepare BiOCl/m-BiVO₄ under mild conditions. Herein, a novel and simple method namely ionic liquid assisted ultrasonic method was developed to prepare BiOCl/m-BiVO₄ heterojunctions in one step at room temperature in a short time via combining the advantages of both of ILs and ultrasound. The ionic liquid 1-butyl-3-methylimidazolium chloride ([BMIM]Cl) and K₆V₁₀O₂₈·9H₂O were acted as a Cl and V source, respectively. And the photocatalytic activities of the as-synthesized BiOCl/m-BiVO₄ heterojunctions were tested via the degradation of Rhodamine B (RhB) under visible light irradiation and sunlight irradiation. The results suggest that BiOCl/m-BiVO₄ heterojunctions exhibited higher photocatalytic activity and stability for the degradation of RhB. Moreover, a possible photocatalytic mechanism has been proposed.

Experimental Section

2.1. Preparation of BiOCl/m-BiVO₄ heterojunctions

All of the chemicals were used as received without further purification. A typical synthetic procedure was as follows. The ionic liquid 1-butyl-3-methylimidazolium chloride ([BMIM]Cl) was added to the water solution (20 mL) of Bi(NO₃)₃·5H₂O (2.42 g, 5 mmol) and K₆V₁₀O₂₈·9H₂O (0.644 g, 0.475 mmol). And the mixture was kept stirring for 20 min at room temperature. The precipitate was obtained after under ultrasonic irradiation for 2 h, and then purified by filtration and washing with water and ethanol several times. Finally, the product as a white powder was dried at 70 °C for 12 h.

2.2. Material characterization and analysis

The crystal structure of the prepared samples was characterized by powder X-ray diffraction (XRD) on a D8 ADVNCE apparatus diffractometer at 40 kV and 40 mA with Cu-K α radiation. X ray photoelectron spectroscopy (XPS) was measured on a PHI5300 with a monochromatic Mg K α source to explore the elements on the surface. The morphology of the samples was observed using a JEOL JSM-6700F scanning electron microscope (SEM). Transmission electron microscopy (TEM) and high-resolution electron microscopy (HREM) images were taken using a JEOL JEM-2010 electron microscope. Nitrogen adsorption–desorption isotherms were obtained on a nitrogen adsorption apparatus (TRISTAR II3020, USA). UV-vis diffuse reflectance spectra were obtained for the dry pressed disk samples with a UV-visible spectrophotometer (UV-2550, Shi-madzu, Japan) using BaSO₄ as a reference. The spectra were recorded at room temperature in the range of 200–800 nm.

2.3. Photocatalytic activity tests

Photocatalytic activities of the products (50 mg) were evaluated by the degradation of RhB solution (2×10^{-5} M, 50 mL). The photocatalytic reaction was conducted under visible light (a 350-W Xe lamp equipped with a 400 nm cut-off filter) and sunlight (Xiangtan, China, 14:30–16:30, 2014/07/10) irradiation for a period time. To eliminate the adsorption/desorption equilibrium effects of RhB and QB, all of the samples were magnetically stirred in dark for 30 min before the irradiation. The solution (4 mL) was taken out periodically and centrifuged to remove the catalysts. The UV-visible absorption spectra were recorded on a Lambda 25 UV-vis spectrophotometer (Perkin-Elmer, USA). The maximum absorption peak of RhB and QB were at 553 nm and 638 nm, respectively, which were used to detect the degradation of RhB and QB. The spectra scan range was 300–800 nm.

Results and discussion

3.1. Structural characterization

As can be seen in Experimental section, the synthetic procedure was very simple. First, the effect of the ionic liquid on the structures of heterojunctions was investigated. And the detailed conditions are available in Table 1. From Fig. 1, it can be seen that all the peaks of the sample S1 are readily indexed to the m-BiVO₄ (JCPDS NO. 39-0256), suggesting that m-BiVO₄ was obtained when no ionic liquid was added. The coexistence of Bi₂WO₆ and BiOCl was observed in samples S2, S3, S4 and S5 with the addition of 1 g, 2 g, 3 g, 4 g [BMIM]Cl, respectively. The XRD patterns of samples S2, S3, S4 and S5 suggest that BiOCl/m-BiVO₄ heterojunctions were well crystallized, and no characteristic peaks of other impurities and undecomposed reactants are observed, demonstrating that the BiOCl/m-BiVO₄ heterojunction is only composed of monoclinic BiVO₄ and tetragonal BiOCl. When increase the amount of [BMIM]Cl to 5 g, the structure of the tetragonal phase of BiOCl (JCPDS No. 06-0249) still existed, while the XRD peaks of BiVO₄ disappeared. These results suggest that the amount of ionic liquid has a significant effect on the structures of the obtained samples and the structures of the BiOCl/m-BiVO₄ heterojunctions can be conveniently controlled via the change of amount of ionic liquid during preparation. To be mentioned, the amount of [BMIM]Cl has a significant effect on the diffraction peak of (110) at $2\theta = 32.5^\circ$. The spacing of (110) planes of S4 show more strong diffraction than that of other samples.

Table 1 The reaction conditions for the samples synthesis.

Sample	Mass of [BMIM]Cl (g)	Products
S1	0	m-BiVO ₄
S2	1.0	BiOCl/m-BiVO ₄
S3	2.0	BiOCl/m-BiVO ₄
S4	3.0	BiOCl/m-BiVO ₄
S5	4.0	BiOCl/m-BiVO ₄
S6	5.0	BiOCl

The mass of Bi(NO₃)₃•5H₂O and K₆V₁₀O₂₈•9H₂O were 2.42 g and 0.644 g, respectively.

To elucidate the surface compositions and chemical states, S4 was chosen as a model for the XPS analysis, and the results are shown in Fig. 2. The peak of C1s at 284.6 eV can be attributed to the carbon contained in the instrument, which was used for calibration.³⁷ Two peaks at 166.7 and 158.8 eV, are attributed to Bi4f5/2 and Bi4f7/2, respectively, which

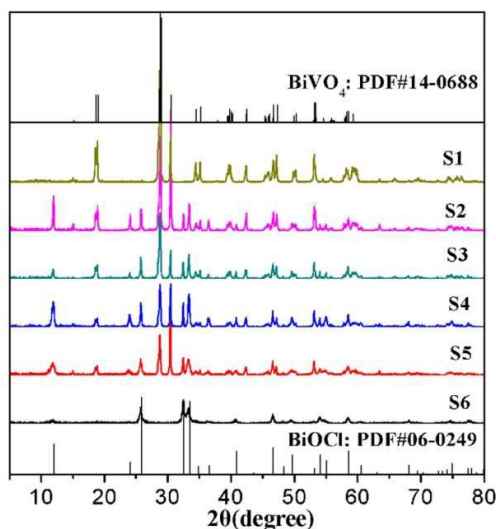


Fig. 1 XRD patterns of BiOCl/ m-BiVO₄ heterojunctions prepared via ionic liquid assisted ultrasonic method.

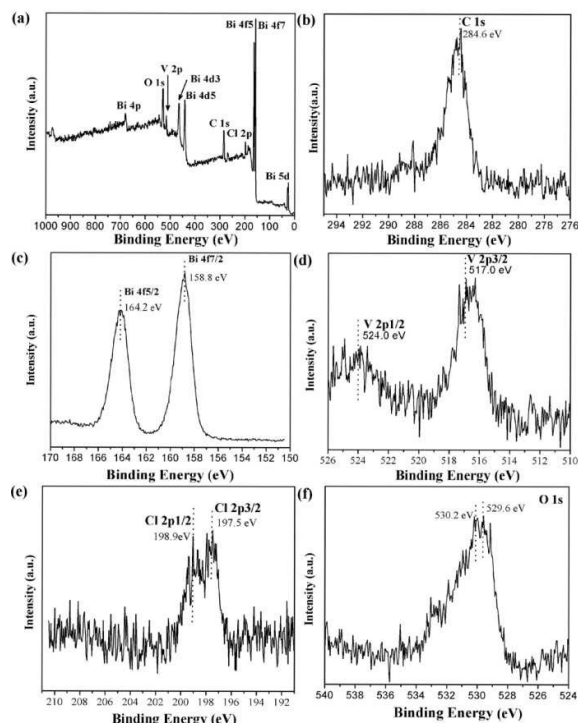


Fig. 2 XPS patterns of the as-prepared BiOCl/m-BiVO₄ heterojunction: (a) typical XPS survey, (b) C1s, (c) Bi4f, (d) V2p, (e) Cl2p and (f) O1s spectra.

confirms that the Bi³⁺ in the BiOCl/m-BiVO₄ heterojunction.³⁸ The characteristic signals of V⁵⁺ in BiVO₄ were observed at 524.9 and 517.3 eV, which corresponds to V2p1/2 and V2p3/2, respectively.³⁷ Cl2p peaks are founded at approximately 198.9 and 197.5 eV, which can be attributed to the Cl 2p1/2 and Cl2p3/2, respectively.³⁹ The O1s peaks for the BiOCl/m-BiVO₄ heterojunction are shown in Fig. 2f, which can be fitted into 529.60 eV and 530.20 eV. The peak at 529.6 eV can be ascribed to the Bi–O bonds,⁴⁰ while the peak centered at 530.20 eV could be assigned to the coordination of oxygen in V–O.⁴¹ The results of XPS analysis are consistent with the result of XRD analysis, and further confirm the coexistence of BiOCl and BiVO₄ in the BiOCl/m-BiVO₄ heterojunction.

The surface morphology of the as-prepared samples was examined by scanning electron microscopy. And the results are shown in Fig. 3. From Fig 3a, it can be seen that the pure m-BiVO₄ consisted of a large number of irregular nanoplates with smooth surfaces. Although there were some differences in morphology and microstructure, the samples of S2, S3 and S5 appeared as square blocks with approximately diameters. Comparing with the samples of S2, S3 and S5, the square blocks in the sample S4 was thin. Obviously, all square blocks are self-assembled by numerous nanoplates, and the average thickness of BiOCl/m-BiVO₄ nanoplates is about 10–20 nm. Fig. 3f displays the SEM images of pure BiOCl (S6), where it can be seen that the morphology of as-prepared BiOCl presents irregular aggregates of uniform nanoparticles.

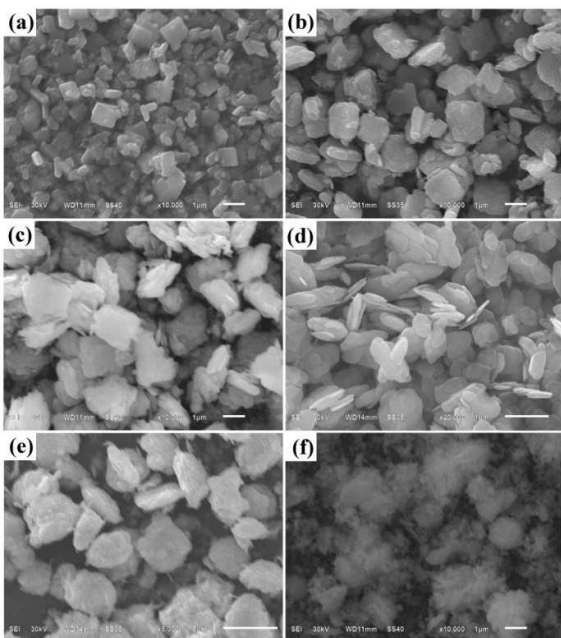


Fig. 3 SEM images of (a) S1, (b) S2, (c) S3, (d) S4, (e) S5, (f) S6 of BiOCl/m-BiVO₄ heterojunction samples.

3.2. TEM and EDS

More detailed structural information of the BiOCl/m-BiVO₄ heterojunction was further investigated by TEM and HRTEM. Fig. 4 shows the TEM images of the BiOCl/m-BiVO₄ (S4) heterojunction. The TEM images in Fig. 4a and 4c show blocks morphology and all blocks consist of large-scale nanoplates with an average width of 100–500 nm and a thickness of 10–200 nm, which is consistent with the SEM observation. Fig. 2c shows a larger number of nanoparticles with a diameter about 5–10 nm were loaded on the nanoplates. Furthermore, the HRTEM images of these nanoparticles was shown in Fig. 4d, which present that the lattice fringes with *d* spacing of 0.344 nm was observed. The lattice interlinear spacing of 0.344 nm is corresponding to the (101) crystal plane of BiOCl, indicating

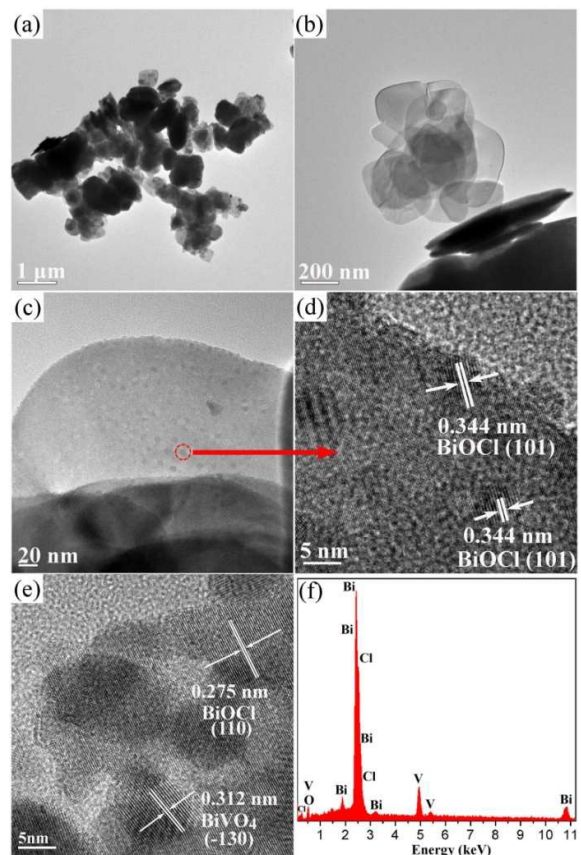


Fig. 4 (a) TEM (a, b, c) and HRTEM (d, e) images of BiOCl/m-BiVO₄ heterojunction, (f) EDS of BiOCl/m-BiVO₄ (S4) heterojunction.

that the nanoparticles are consist of BiOCl. In Fig. 4e, the lattice interlinear spacing of 0.275 and 0.312 nm coincide with the (110) crystal plane of the tetragonal BiOCl and the (-130) crystal plane of m-BiVO₄, respectively. The above results suggest that the intimate interfaces between BiOCl and m-BiVO₄ in the heterojunction were successfully constructed. Fig. 4e shows the EDS spectrum of S4, the corresponding peaks of Bi, V, O and Cl element can be detected, which further confirms that the as-prepared samples are formation of a heterojunction at the contact interface of BiOCl and m-BiVO₄.

3.3. UV–Vis Diffuse Reflectance Spectroscopy

The band gap energy of a semiconductor is a key factor in determining its photoabsorption and photocatalytic performance. Fig. 5a shows the UV–vis diffuse reflectance spectra of the as-prepared samples. It can be seen that the absorption edge of pure m-BiVO₄ (S1) is at 530 nm approximately. And the band-gap energy of m-BiVO₄ (S1) was estimated via the formula $\alpha h\nu = A(h\nu - E_g)^{n/2}$, where α , ν , E_g and A are an absorption coefficient, a light frequency, the band gap, and a constant, respectively.⁴¹ Among them, n is a constant, which depended by the characteristics of optical transition in the semiconductor ($n = 1$ for direct transition and $n = 4$ for indirect transition). For m-BiVO₄

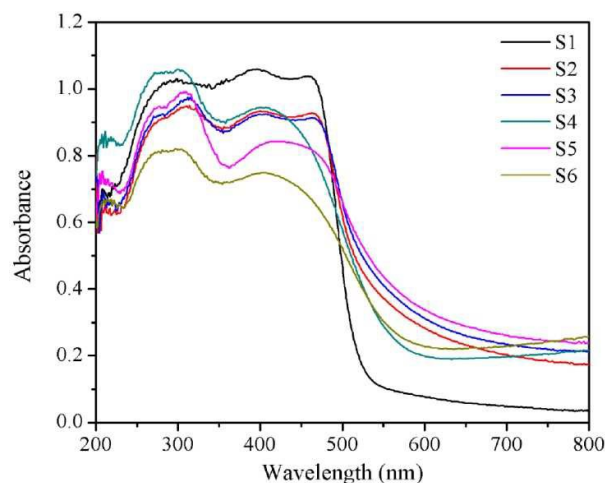


Fig. 5 UV-vis diffuse reflectance spectra of samples.

semiconductor, n is 1. The E_g was obtained from the intercepts of the $(\alpha h\nu)^{2/n}$ versus photon energy ($h\nu$) plots. Therefore, the band-gap energy was calculated to be 2.48 eV for $m\text{-BiVO}_4$ (S1). As we all known, the white BiOCl does not have any absorption in the visible light range, while the pale yellow BiOCl (S6) has absorption in the spectra of visible light range, due to that the surfaces of BiOCl (S6) nanocrystals became disordered, leading to the intraband transitions between the impurity level and the conduction band instead of the intrinsic transition from the valence band to the conduction band.⁴² Compared with the $m\text{-BiVO}_4$ nanostructures, the absorption edge of $\text{BiOCl}/m\text{-BiVO}_4$ (S2, S3, S4 and S5) heterojunctions slightly increases, probably due to quantum-size effects resulting from the nanoparticles among the nanoplates. All $\text{BiOCl}/m\text{-BiVO}_4$ heterojunctions have visible light photoabsorption abilities and lead to a lower band gap, which is helpful for electronic transition and exciting more active species. Therefore, $\text{BiOCl}/m\text{-BiVO}_4$ heterojunctions may enhance visible light photocatalytic activity.

3.4. BET surface areas and pore size distributions

Brunauer-Emmett-Teller (BET) specific surface areas of the as-prepared samples were investigated by nitrogen adsorption-desorption isotherms. As shown in Fig. 6, the adsorption-desorption isotherms of all samples could be categorized as type IV isotherm with a type of H3 hysteresis loop (at $p/p_0 = 0.8\text{-}1.0$), which indicates the presence of mesopores (2–50 nm in size).⁴³ Moreover, the hysteresis loop of the adsorption-desorption isotherms of S4, S5 and S6 shift approach $p/p_0 = 1$, suggesting the existence of macropores (>50 nm) in S4, S5 and S6.⁴⁴ The pore-size distributions of all samples are available in Fig. S1 in Supporting Information,

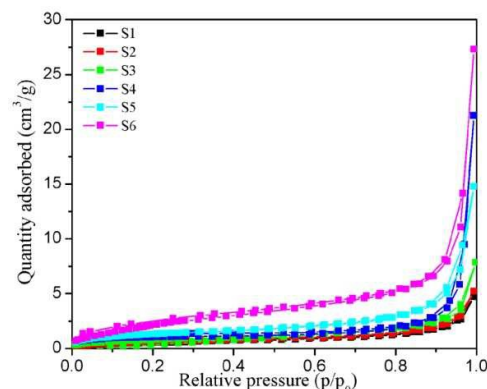


Fig. 6 Nitrogen adsorption-desorption isotherms of samples.

Table 2 BET Surface Area, total pore volume and average pore size of samples.

Sample	S_{BET} (m^2g^{-1})	Total pore volume (cm^3/g)	Average pore size (nm)
S1	1.95	0.0074	14.84
S2	2.10	0.0076	15.15
S3	2.69	0.0118	15.32
S4	4.00	0.0322	42.35
S5	5.07	0.0222	23.01
S6	8.03	0.0413	19.02

further confirming the foregoing results. The data of S_{BET} and pore parameters of as-prepared are presented in Table 2. The BET surface area increases with the increase of $[\text{BMIM}]\text{Cl}$, which may be attributed to that more $[\text{BMIM}]\text{Cl}$ resulted in more BiOCl nanoparticles in the heterojunction. The result is consistent with the SEM images.

3.5. Photocatalytic performance

The photocatalytic activities of the as-synthesized samples were evaluated by the degradation of RhB as a model pollutant under visible light and sunlight irradiation. Fig. 7a shows the concentration variation of RhB with reaction time. It is about 3.0% RhB degradation in the blank experiment without photocatalyst, indicating that the self-photolysis of RhB could almost be neglected. After 180 min of visible light irradiation, the photodegradation efficiencies of RhB are 16%, 8%, 12% and 99% for S1, S2, S3 and S4, respectively. However, S5 and S6 only have certain adsorptivity, and the photodegradation efficiencies were almost not changed under visible light irradiation. Hence, the S4 has the highest efficiency for the photodegradation of RhB under visible light. Fig. 7b presents the UV-vis absorption spectrum of RhB solution with S4 as the photocatalyst at different irradiation time. The absorption peak gradually blue shifted with the increase of irradiation time, which may due to that RhB was demethylated and then the conjugated structure was degraded under visible light irradiation.

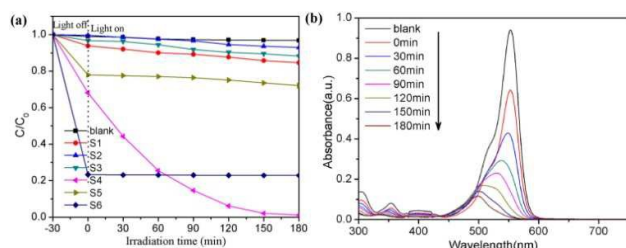


Fig. 7 (a) Time-course variation of C/C_0 of RhB solution under visible light irradiation in the presence of the as-prepared samples; (b) UV-vis absorption spectra of RhB solution after being treated with S4 as photocatalyst under visible light irradiation.

Sunlight is a renewable energy and can be got freely. Hence, the investigation of pollutants degradation under sunlight has a great significant effect on both resource and environment. Herein, the degradation of RhB in the presence of the above as-prepared samples was also tested under the irradiation of sunlight at room temperature, and the results are shown in Fig. 8. The results were similar with that under the visible light irradiation. The S6 only has adsorptivity. And after under sunlight irradiation for 120 min, the photodegradation efficiencies of RhB are 69%, 15%, 20%, 98% and 33% for S1, S2, S3, S4 and S5, respectively, indicating the

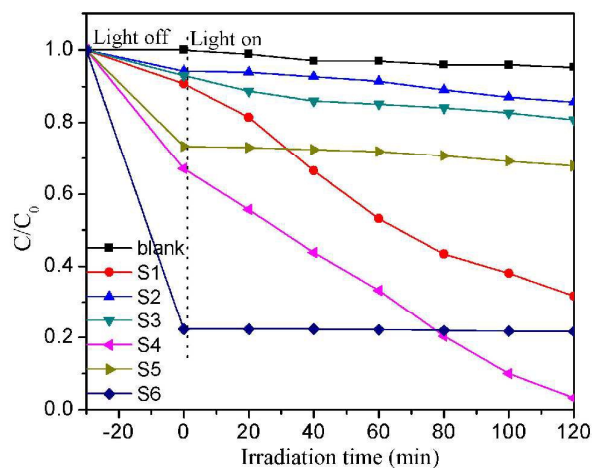


Fig. 8 Time-course variation of C/C_0 of RhB solution under sun light irradiation in the presence of the as-prepared samples.

S4 shows the highest photocatalytic ability. On the other hand, it can be seen that the degradation rate under sunlight irradiation was faster than that under visible light irradiation. Therefore, the sunlight can act as an available light source for the photocatalytic degradation of pollutants.

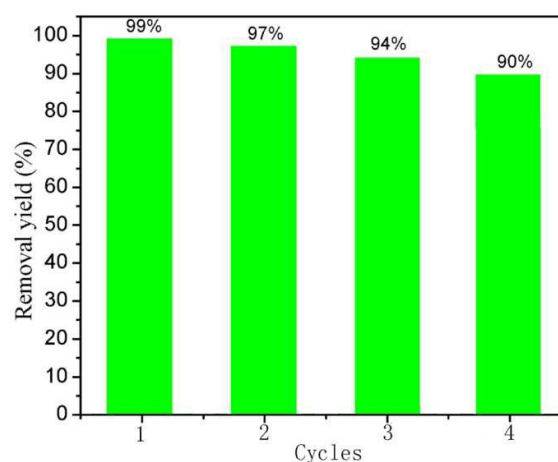


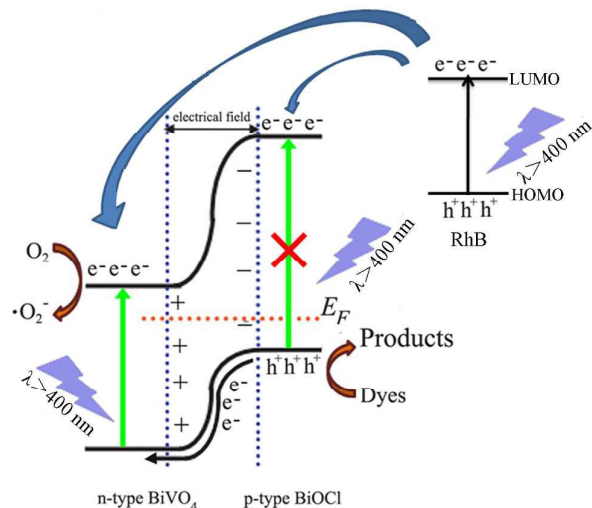
Fig. 9 Recycling experiments for degradation of RhB with BiOCl/m-BiVO₄ (S4) as a photocatalyst under visible light irradiation.

To evaluate the stability and reusability of the BiOCl/m-BiVO₄ heterojunctions, the recycling experiments were conducted for the degradation of RhB with S4 as the photocatalyst under visible light irradiation. As shown in Fig. 9, the photodegradation efficiency of RhB decreases from 99% to 90% after four cycles, indicating that the as-prepared BiOCl/m-BiVO₄ heterojunctions are still stable under visible light irradiation.

3.6. Photocatalytic mechanism

It is well known that photocatalytic degradation of pollutants under light irradiation is mainly based on the generation and separation of the photoelectron-hole pairs. The excited-state e^- or h^+ pairs can react with an electron acceptor or donor to produce radicals such as $\bullet\text{OH}$ and $\bullet\text{O}_2^-$. These radicals are very active, which can oxidize or reduce toxic organic molecules. However, the produced photoelectron-hole pairs in m-BiVO₄ are easily recombined, which induces that less electrons and holes are generated to react with O_2 and H_2O to produce active radical species, as a result, the degradation activity is weak. The coupling of BiVO₄ with BiOCl can effectively generate and separate e^-/h^+ pairs and enhance photocatalyst activity. As shown in Scheme 1, a possible mechanism of the charge separation and transfer in the BiOCl/m-BiVO₄ heterojunctions under visible light irradiation was proposed. BiOCl is a p-type semiconductor,⁴⁵ while m-BiVO₄ is an n-type semiconductor.⁴⁶ When BiVO₄ contact with BiOCl, an internal static electric field is formed at the interface between them, and the BiOCl/m-BiVO₄ p-n junction will be formed when their Fermi levels (E_F) reached equilibrium state. With the visible light or sunlight irradiation (the wavelength of 400 nm corresponds to energy of 3.1 eV), the electrons on the valence band (VB) of m-BiVO₄ can be excited to the conduction band (CB), due to the higher photon energy. However, the E_g of BiOCl is larger than 3.1 eV,⁴⁷ so BiOCl cannot be activated. As we all know, the electric field at the interface facilitates the migration of electrons from the VB of the p-type semiconductor to the VB of the n-type semiconductor. Therefore, the electrons in the VB of BiOCl

could easily be transferred to the VB of BiVO_4 . Meanwhile, holes are generated in the VB of BiOCl . On the other hand, the electrons in the HOMO of RhB can be excited to the LUMO of RhB under visible light irradiation.⁴⁸ Due to the large offset of energy level at the RhB/ BiVO_4 interfaces, photogenerated electrons move rapidly from RhB to BiVO_4 in a thermodynamically favorable manner. In above way, photoinduced electron-hole pairs could be effectively separated. Moreover, the holes in the VB of BiOCl could initiate photocatalytic oxidation reactions, and the excited electrons in the CB of BiVO_4 photogenerated electrons can react with O_2 to form $\bullet\text{O}_2^-$ radicals.



Scheme 1 A possible mechanism of the charge separation and transfer in the $\text{BiOCl}/\text{m-BiVO}_4$ heterojunctions under visible-light irradiation.

Therefore, $\text{BiOCl}/\text{m-BiVO}_4$ heterostructures could exhibit better photocatalytic properties than that of BiOCl and m-BiVO_4 on degradation of pollutants. In this study, the S4 heterostructure exhibits the best photocatalytic activity. It is straightforward to assume that the larger pore volume and pore size of S4 are helpful for increasing the adsorbability, leading to the e^- in the LUMO levels of dyes more easily transfer to the CB of BiVO_4 and produce more $\bullet\text{O}_2^-$ radicals under visible light irradiation. The other reason for the S4 heterostructure exhibits the best photocatalytic activity could be related to an increase in charge separation. With m-BiVO_4 amount in $\text{BiOCl}/\text{m-BiVO}_4$ being in excess, numerous photoinduced electrons and holes could recombine easily on the surface of m-BiVO_4 . However, when the amount of BiOCl in $\text{BiOCl}/\text{m-BiVO}_4$ is excess, less photoinduced electrons and holes could be generated. Therefore, the certain ratio of BiOCl and m-BiVO_4 in S4 may be helpful to form the maximum number of space charge regions. Comparing with other samples, the spacing of (110) planes of S4 show more strong diffraction. More O_2 can be absorbed and converted to $\bullet\text{O}_2^-$, due to the existence of the strong diffraction of (110).⁴⁹ Therefore, the high exposure of (110) plane may lead to more better photocatalytic activity of S4.⁵⁰

Conclusions

In summary, a novel and simple method namely ionic liquid assisted ultrasonic method was developed to prepare $\text{BiOCl}/\text{m-BiVO}_4$ heterojunctions at room temperature. The ionic liquid $[\text{BMIM}]\text{Cl}$ and the salt $\text{K}_6\text{V}_{10}\text{O}_{28}\cdot 9\text{H}_2\text{O}$ were acted as Cl and V source, respectively. A series of characterization methods were used to characterize the synthesized $\text{BiOCl}/\text{m-BiVO}_4$ heterojunctions. The as-prepared heterostructures are composed of BiOCl nanoparticles growing on the BiVO_4 nanoplates. The photocatalytic activities of the as-synthesized $\text{BiOCl}/\text{m-BiVO}_4$ heterostructures products were tested via the degradation of dyes under visible light irradiation and sunlight irradiation. Due to the larger adsorbability, high exposure of (110) planes and suitable conduction and valence band levels of BiVO_4 and BiOCl , the S4 heterojunctions possessed significantly enhanced photocatalytic activities under visible light and sunlight irradiation. Considering the high photocatalytic efficiency and stability, with further improvement and optimization, the $\text{BiOCl}/\text{m-BiVO}_4$ heterojunction photocatalysts has potential application in environmental purification.

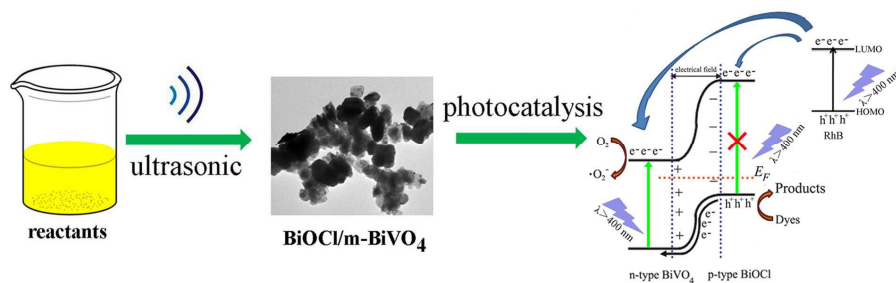
Acknowledgements

The authors acknowledge with thanks the financial support of the Provincial Natural Science Foundation of Hunan, China (2015JJ2138), the Open Project Program of State Key Laboratory of Structural Chemistry, China (No. 20150018) and the National Natural Science Foundation of China (21343008).

Notes and references

- L. Q. Ye, K. J. Deng, F. Xu, L. H. Tian, T. Y. Peng and L. Zan, *Phys. Chem. Chem. Phys.*, 2012, **14**, 82.
- W. F. Yao, X. H. Xu, H. Wang, J. T. Zhou, X. N. Yang, Y. Zhang, S. X. Shang and B. B. Huang, *Appl. Catal. B: Environ.*, 2004, **52**, 109.
- D. Chatterjee and A. Mahata, *Appl. Catal. B: Environ.*, 2001, **33**, 119.
- T. E. Doll and F. H. Frimmel, *Catal. Today*, 2005, **101**, 195.
- Z. J. Zhou, M. C. Long, W. M. Cai and J. Cai, *J. Mol. Catal. A: Chem.*, 2012, **353–354**, 22.
- L. Zhang, D. R. Chen and X. L. Jiao, *J. Phys. Chem. B*, 2006, **110**, 2668.
- S. W. Cao, Z. Yin, J. Barber, F. Y. C. Boey, S. C. J. Loo and C. Xue, *ACS Appl. Mater. Interfaces*, 2011, **4**, 418.
- C. Karunakaran, S. Kalavani and P. Vinayagamorthy, *Mater. Lett.*, 2014, **122**, 21.
- M. Wang, Y. Che, C. Niu, M. Dang and D. Dong, *J. Hazard. Mater.*, 2013, **262**, 447.
- Y. S. Fu, X. Q. Sun and X. Wang, *Mater. Chem. Phys.*, 2011, **131**, 325.
- L. Ren, L. Jin, J. B. Wang, F. Yang, M. Q. Qiu and Y. Yu, *Nanotechnology*, 2009, **20**, 115603.
- W. Yin, W. Wang, M. Shang, L. Zhou, S. Sun and L. Wang, *J. Inorg. Chem.*, 2009, **29**, 4379.
- L. Ge, *Mater. Chem. Phys.*, 2008, **107**, 465.
- A. P. Zhang and Z. J. Zhang, *Appl. Surf. Sci.*, 2010, **256**, 3224.
- L. Li and B. Yan, *J. Alloy. Compd.*, 2009, **476**, 624.
- Z. He, Y. Shi, C. Gao, L. Wen, J. Chen and S. Song, *J. Phys. Chem. C*, 2014, **118**, 389.

- 17 Z. Y. Wang, B. B. Huang, Y. Dai, X. Y. Qin, X. Y. Zhang, P. Wang, H. X. Liu and J. X. Yu, *J. Phys. Chem. C*, 2009, **113**, 4612.
- 18 S. Y. Chai, Y. J. Kim, M. H. Jung, A. K. Chakraborty, D. Jung and W. I. J. Lee, *Catal.*, 2009, **262**, 144.
- 19 L. Li and B. Yan, *J. Alloy. Compd.*, 2009, **476**, 624.
- 20 J. Su, X. X. Zou, G. D. Li, X. Wei, C. Yan, Y. N. Wang, J. Zhao, L. J. Zhou and J. S. Chen, *J. Phys. Chem. C*, 2011, **115**, 8064.
- 21 P. Madhusudan, J. R. Ran, J. Zhang and G. Liu, *Appl. Catal. B: Environ.*, 2011, **110**, 286.
- 22 W. Zhao, Y. Wang, Y. Yang, J. Tang and Y. N. Yang, *Appl. Catal. B: Environ.*, 2012, **115**, 90.
- 23 D. Q. Zhang, M. C. Wen, B. Jiang, G. S. Li and J. C. Yu, *J. Hazard. Mater.*, 2012, **211**, 104.
- 24 J. M. Ma, X. D. Liu, J. B. Lian, X. C. Duan and W. J. Zheng, *Cryst. Growth Des.*, 2010, **10**, 2522.
- 25 M. L. Guan, D. K. Ma, S.W. Hu, Y. J. Chen and S. M. Huang, *Inorg. Chem.*, 2011, **50**, 800.
- 26 J. D. Oxley, T. Prozorov and K. S. Suslick, *J. Am. Chem. Soc.*, 2003, **125**, 11138.
- 27 W. B. McNamara, Y. T. Didenko and K. S. Suslick, *Nature*, 1999, **401**, 772.
- 28 U. Pal, C. W. Kim, N. A. Jadhav and Y. S. Kang, *J. Phys. Chem. C*, 2009, **113**, 14676.
- 29 J. J. Guo, S. M. Zhu, Z. X. Chen, Y. Li, Z. Y. Yu, Q. L. Liu, J. B. Li, C. L. Feng and D. Zhang, *Ultrason. Sonochem.*, 2011, **18**, 1082.
- 30 A. Gedanken, *Ultrason. Sonochem.*, 2004, **11**, 47.
- 31 N. A. Dhas and A. Ekhtiarzadeh, *J. Am. Chem. Soc.*, 2001, **123**, 8310.
- 32 Z. Ma, J. H. Yu and S. Dai, *Adv. Mater.*, 2010, **22**, 261.
- 33 J. Dahl, B. L. S. Maddux and J. E. Hutchison, *Chem. Rev.*, 2007, **107**, 2228.
- 34 M. Antonietti, D.B. Kuang, B. Smarsly and Z. Yong, *Angew. Chem. Int. Ed.*, 2004, **43**, 4988.
- 35 Z. Q. He, Y. Q. Shi, C. Gao, L. N. Wen, J. M. Chen and S. Song, *J. Phys. Chem. C*, 2014, **118**, 389.
- 36 J. Cao, C. C. Zhou, H. L. Lin, B. Y. Xu and S. F. Chen, *Appl. Surf. Sci.*, 2013, **284**, 263.
- 37 M. C. Long, W. M. Cai, J. Cai, B. X. Zhou, X. Y. Chai and Y. H. Wu, *J. Phys. Chem. B*, 2006, **110**, 20211.
- 38 K. L. Zhang, C. M. Liu, F. Q. Huang, C. Zheng and W. D. Wang, *Appl. Catal. B: Environ.*, 2006, **68**, 125.
- 39 F. Dong, Y. J. Sun, M. Fu, Z. B. Wu and S. C. Lee, *J. Hazard. Mater.*, 2012, **219**, 26.
- 40 M. S. Gui, W. D. Zhang, Q. X. Su and C. H. Chen, *J. Solid State Chem.*, 2011, **184**, 1977.
- 41 S. Wu, H. Zheng, Y. Lian and Y. Wu, *Mater. Res. Bull.*, 2013, **48**, 2901.
- 42 X. Chen, L. Liu, P. Y. Yu, S. S. Mao, *Science*, 2011, **331**, 746.
- 43 L. P. Zhu, G. H. Liao, N. C. Bing, L. L. Wang, Y. Yang and H. Y. Xie, *CrystEngComm*, 2010, **12**, 3791.
- 44 T. B. Li, G. Chen, C. Zhou, Z. Y. Shen, R. C. Jin and J. X. Sun, *Dalton Trans.*, 2011, **40**, 6751.
- 45 C. R. Michel, N. L. L. Contreras and A. H. Martínez-Preciado, *Sensor. Actuat. B: Chem.*, 2011, **160**, 271.
- 46 W. R. Zhao, Y. Wang, Y. Yang, J. Tang, Y. N. Yang, *Appl. Catal. B: Environ.*, 2012, **115**, 90.
- 47 K. Zhang, C. Liu, F. Huang, C. Zheng, W. Wang, *Appl. Catal. B: Environ.*, 2006, **68**, 125.
- 48 M. Xiong, L. Chen, Q. Yuan, J. He, S. L. Luo, C. T. Au and S.F. Yin, *Dalton Trans.*, 2014, **43**, 8331.
- 49 M. Setvín, U. Aschauer, P. Scheiber, Y. F. Li, W. Y. Hou, M. Schmid, A. Selloni, U. Diebold, *Science*, 2013, **341**, 988.
- 50 L. Chen, S. F. Yin, R. Huang, Y. Zhou, S. L. Luo, C. T. Au, *Catal. Commun.*, 2012, **23**, 54.



Ionic liquid assisted ultrasonic method was developed to prepare BiOCl/m-BiVO₄ heterojunctions with high photocatalytic activity under both visible light and sunlight irradiation.